Photodissociation of Solvated Metal Cation Complexes $Mg^+(OCNC_2H_5)_n$ ($n = 1-3$)

Ju-Long Sun,[†,‡] Haichuan Liu,[†] Hong-Ming Yin,[‡] Ke-Li Han,[*,‡] and Shihe Yang[*,†]

Department of Chemistry, The Hong Kong University of Science and Technology, Clear Water Bay, Kowloon, Hong Kong, China, and State Key Laboratory of Molecular Reaction Dynamics, Dalian Institute of Chemical Physics, Chinese Academy of Sciences, 457 Zhongshan Road, 116023 Dalian, China

Received: December 31, 2003; In Final Form: February 24, 2004

Ethyl isocyanate-solvated magnesium cation complexes $Mg^+(OCNC_2H_5)_n$ were produced in a laser-ablation supersonic expansion nozzle source. Photoinduced reactions in the complexes of $Mg^+(OCNC_2H_5)_n$ ($n = 1-3$) have been studied as a function of the number of solvent molecules. Photodissociation action spectra of $Mg^+(OCNC_2H_5)_{1-3}$ were recorded in the spectral range of 230−440 nm. Except for minor reactive products $C_2H_5^+$ and Mg^+OCN at short wavelengths from the photoreaction of the singly solvated complex $Mg^+(OCNC_2H_5)$, only evaporation products were observed from photodissociation of $Mg^+(OCNC_2H_5)_n$ ($n = 1-3$). For all three complexes we studied, the ligands are believed to be in the first solvation shell. The action spectra of $Mg^+(OCNC_2H_5)_{1-3}$ consist of two or three peaks on the red and blue sides of the Mg^+ $3\,^2P \leftarrow 3\,^2S$ atomic transition. The ground-state geometries of $Mg^+(OCNC_2H_5)_{1-3}$ were fully optimized at the B3LYP/6-31+G** level by using the GAUSSIAN 98 package. The absorption spectra of the complexes $Mg^+(OCNC_2H_5)_{1-3}$ were calculated by using the optimized structures of their ground states with the CIS/6-31+G** method. The theoretical predictions appear to be consistent with the experimental results. An sp hybridization mechanism was proposed for the complexation of Mg^+ and $OCNC_2H_5$, which results in the formation of big π bonds between the magnesium cation and the ethyl isocyanate molecule, and further rationalizes the nearly linear backbone of $Mg^+-O-C-N-C$ in the complex $Mg^+(OCNC_2H_5)$.

1. Introduction

Photodissociation of clusters has been the focus of many investigations[1−18] because clusters represent a "fifth state of matter" holding promise for "bridging the gap" between the gas and condensed phase.[19−22] Ion solvation plays an important role in biological, chemical, and physical processes.[1−8] Clusters containing metal ions and solvent molecules present an ideal model system for understanding how the metal ions are solvated by the solvent molecules.[9−18] Singly charged alkaline earth metal cations have an open-shell structure and are isoelectronic to the alkali metal atoms. They have substantial oscillator strengths in the ultraviolet spectral regions, which can be easily accessed by pulsed laser sources. With the rapid development of the techniques in supersonic expansion, time-of-flight mass spectrometry, and laser spectroscopy, much work has been directed on the photodissociation of the alkaline-earth cation−molecule complexes. Photodissociation studies on Mg^+ and Ca^+ solvated by H_2O were performed by Fuke et al.[11,23] They found that the photodissociation action spectra of $Mg^+(H_2O)_n$ ($n = 1-5$) and $Ca^+(H_2O)_n$ ($n = 1-6$) exhibited the trend of shifting to lower energies with an increasing number of ligands. Duncan et al.[13,24] performed photodissociation studies on Mg^+ and Ca^+ solvated by H_2O and D_2O. They measured many of the vibrational frequencies for the $^2B_2$ and $^2B_1$ excited states (based on C_{2v} symmetry). The experimental data are in good agreement with the ab initio calculations.[14,25] Farrar's group studied the systems of $Sr^+(NH_3)_n$ ($n = 1-6$), $Sr^+(H_2O)_n$ ($n = 1-4$), and $Sr^+(D_2O)_n$ ($n = 1-6$).[4,15,26] For the photodissociation of $Sr^+(H_2O)_n$ and $Sr^+(D_2O)_n$, both ligand loss products and H/D elimination products were identified. However, all fragment ions after the photodissociation of $Sr^+(NH_3)_n$ were found to be from the sequential evaporation. Recently, our group studied the photodissociation of $Mg^+(FCH_3)_n$ ($n = 1-4$).[18] In complexes with successive solvation, the observed photodissociation channels and action spectra vary dramatically with the number of solvent molecules.

Many experimental and theoretical studies have been focused on isocyanates due to the interesting NCO functional group.[27−32] The formation and identification of NCO-containing species as well as the NCO migration are of significant value in transition metal catalytic reactions.[33−39] Very recently, our group studied the photodissociation of $Mg^+(NCCH_3)_n$ ($n = 1-4$).[8] Because CH_3CN possesses a large dipole moment ($\mu = 3.92$ D), the electrostatic interaction between the magnesium cation and acetonitrile is apparently enhanced. In CH_3CN, the lone-pair electrons of the N atom and the π and π^* orbitals of the N≡C group interact with the three 3p orbitals of Mg^+, resulting in some interesting spectroscopic and dynamic features of the complex. In C_2H_5NCO, the O atom also possesses lone-pair electrons just as the N atom does. In addition, the π system of NCO is substantially different from that of N≡C. One would thus expect different intermolecular interactions between the magnesium cation and ethyl isocyanate complex. In this paper, we continue our previous work[40] by investigating the photoinduced reactions in the binary complex $Mg^+(OCNC_2H_5)$ and report on our solvation studies of $Mg^+(OCNC_2H_5)_n$ ($n = 1-3$). The complexes of $Mg^+(OCNC_2H_5)_n$ were produced in a

* Address correspondence to these authors. K.-L.H.: e-mail klhan@dicp.ac.cn, fax (86) 411-4675584. S.Y.: e-mail chsyang@ust.hk, fax (852) 2358-1594.

† The Hong Kong University of Science and Technology.

‡ Chinese Academy of Sciences.

10.1021/jp0380529 CCC: $27.50
Published on Web 04/14/2004

supersonic expansion nozzle source. The photodissociation action spectra of $Mg^+(OCNC_2H_5)_{1-3}$ were recorded in a broad wavelength range of 230−440 nm. Theoretical calculations were performed on the structures of both the parents and the daughters and used to interpret the observed dissociation channels and action spectra.

2. Experimental Section

The experimental apparatus has been depicted previously[41] and thus only the parts relevant to the present experiments are given here. A rotating magnesium rod attached to a sample holder was mounted 15 mm downstream from the exit of a pulsed valve (General Valve). Driven by a step motor, the sample rod rotated on each laser pulse to expose the fresh surface during the laser-ablation experiments. The pulse valve was used to generate ethyl isocyanate clusters by supersonic expansion of a gas mixture of ethyl isocyanate vapor seeded in helium carrier gas (with a backing pressure of 40 psi) through a 0.5 mm diameter orifice. The second harmonic (532 nm) of a pulsed Nd:YAG laser (∼40 mJ/pulse) was weakly focused onto the magnesium rod surface (∼1 mm diameter spot) for generating metal cations. The laser-vaporized species traversed the supersonic jet stream 20 mm from the ablation sample target, forming a series of solvated metal cation−ethyl isocyanate cluster complexes. The clusters thus formed traveled 14 cm downstream to the extraction region of the reflection time-of-flight spectrometer (RTOFMS).

The cation−molecule complexes were accelerated vertically by a high-voltage pulse (∼1000 V in amplitude and 25 μs in width) in a two-stage extractor. The first plate was applied with the full pulser, e.g., ∼1000 V, while the voltage of the second plate was set at 81% for recording mass spectra and at 97% for conducting photodissociation experiments. After extraction, the cation−molecule complexes were steered by a pair of horizontal plates and a pair of vertical deflection plates. The voltages on these plates were set at +500 and −50 V, respectively. All the cluster cations were reflected by the reflectron (VR1 = +650 V and VR2 = +1050 V) and finally detected by a dual-plate microchannel detector (MCP). A two-plate mass gate equipped with a high-voltage pulser (normally high at +500 V) was used to select the $Mg^+(OCNC_2H_5)_n$ ($n = 1-3$) parent clusters. Once the mass-selected cluster cations, $Mg^+(OCNC_2H_5)_n$, arrived at the turn-round region of the reflectron, they were irradiated with a collimated beam of a dye laser. The parent and nascent daughter cations were reaccelerated by the reflectron electric field and detected by the MCP detector. The dye laser for photodissociation was pumped by a XeCl excimer laser (Lambda Physik LPX 210i/LPD 3002). Fundamental outputs (for the dyes including *p*-Terphenyl, DMQ, BBQ, Stilbene 420) and second harmonic outputs (for the dyes including Coumarin 480, Coumarin 503, Coumarin 540A, Kiton Red, and DCM) were used to cover the spectral region between 230 and 440 nm with reasonable wavelength overlaps. The dissociation laser fluence was kept low (<1 mJ/cm^2) to ensure one-photon processes and avoid saturation phenomena.

3. Results and Discussion

3.1. Photodissociation of $Mg^+(OCNC_2H_5)_n$. A typical mass spectrum of magnesium cation−ethyl isocyanate clusters is shown in Figure 1. The metal-bearing mass peaks can be easily identified by the isotope distribution of magnesium. The $Mg^+(OCNC_2H_5)_{n-1}$ cluster species are obviously the association products from the collisions between Mg^+ and $(OCNC_2H_5)_n$, which were produced by the pulsed supersonic nozzle. These

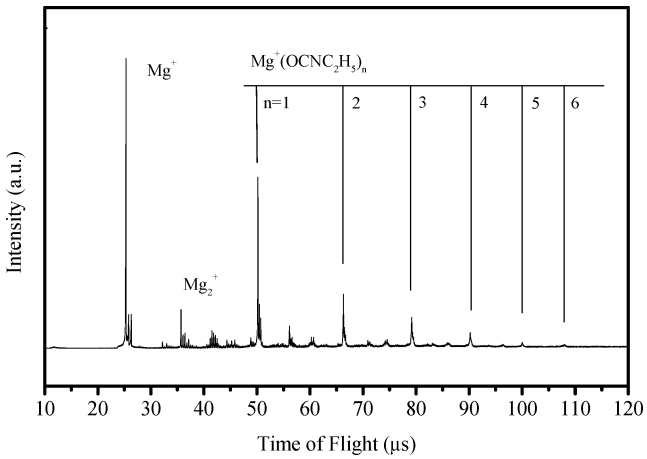

Figure 1. Time-of-flight mass spectrum of the metal cation−molecule complexes $Mg^+(OCNC_2H_5)_n$ from the supersonic expansion nozzle source.

cation−molecule complexes could be stabilized by either a third-body collision or evaporation of a $OCNC_2H_5$ molecule from $(OCNC_2H_5)_n$. As can be seen in Figure 1, the intensity of $Mg^+(OCNC_2H_5)_n$ ($n = 1-6$) decreases monotonically with n increasing and no magic numbers were observed. The largest cluster we were able to observe was $Mg^+(OCNC_2H_5)_6$, although we optimized fully the formation conditions by appropriately setting the delay and length of the gas valve, the amplitude of the pulsed high voltage, and the voltage of the MCP detector. One of the essentials for producing large clusters is to form hydrogen bonds among molecules. For small polar solvent molecules such as H_2O, NH_3, and CH_3OH, at the first step for the formation of cation−molecule complexes, they interact directly with a metal cation, filling the first solvation shell. Then, second or even more shells can be added through hydrogen bonds to form larger clusters. For example, in the photodissociation study on $Mg^+(H_2O)_n$,[14] Fuke et al. observed $n >$ 15 parent clusters. In our previous experiment,[17] cluster $Mg^+(CH_3OH)_n$ with n up to 20 could be identified clearly. However, for the relatively big $OCNC_2H_5$ molecules, it is difficult to form hydrogen bonds among themselves. Therefore, when the first solvation shell is fully filled, it is difficult to form the larger cluster $Mg^+(OCNC_2H_5)_n$.

Theoretical calculations[42] showed that the first solvation shell contains four and eight acetonitrile molecules for $Li^+(NCCH_3)_n$ and $Na^+(NCCH_3)_n$, respectively. Now that the coordination spheres of Li^+ and Na^+ saturate with four and eight acetonitrile molecules, one would expect the number of acetonitrile molecules in the first solvation shell to be larger than eight for $Mg^+(NCCH_3)_n$ due to Mg^+ possessing a larger ionic radius. However, because of the presence of an extra electron in the 3s orbit in Mg^+, the solvation is different from the situation of Li^+ and Na^+ due to their closed shell. Indeed, the photodissociation experiment on $Mg^+(NCCH_3)_n$[8] revealed the number of coordination was less than 7 (e.g., $n < 7$). Although there is no theoretical study on the solvation of $Mg^+(OCNC_2H_5)_n$, by comparison with the theoretical and experimental study on $Mg^+(NCCH_3)_n$ above, we think that the maximum number for the first shell solvent molecules in $Mg^+(OCNC_2H_5)_n$ is no more than 6.

Representative photodissociation difference mass spectra of size-selected $Mg^+(OCNC_2H_5)_n$ ($n = 1-3$) at laser wavelengths of 255, 339, and 414 nm are shown in Figure 2. The difference mass spectra are obtained from the subtraction of the photodissociation mass spectra with the photolysis laser

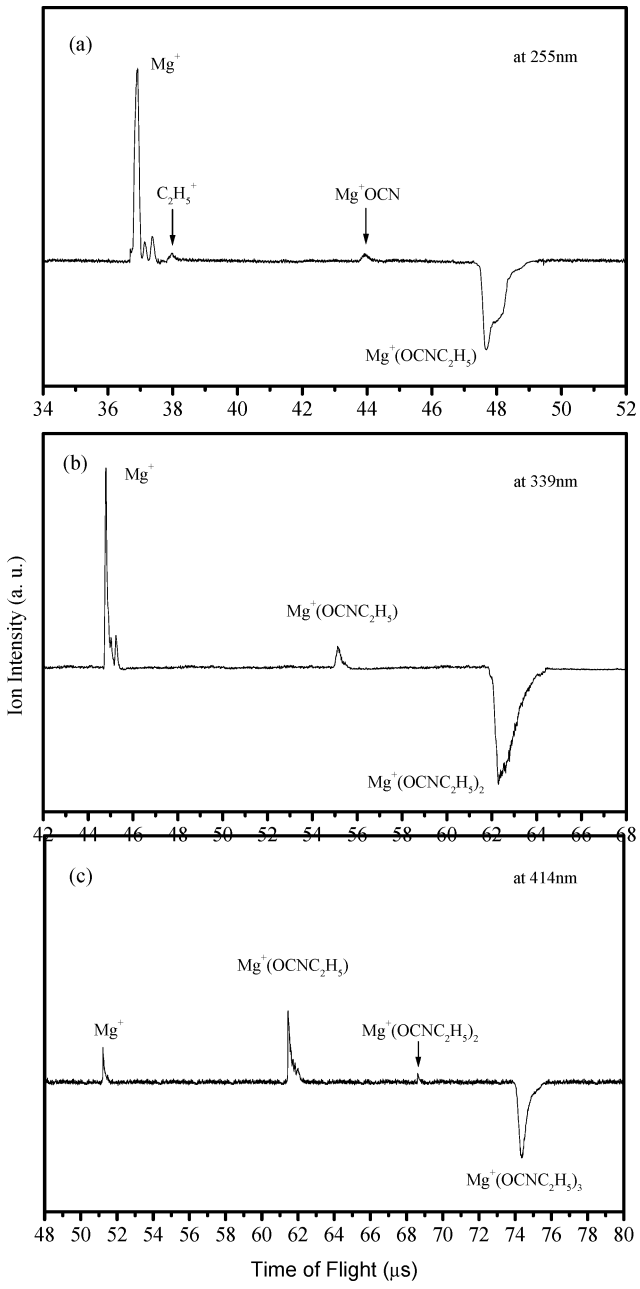

Figure 2. Photodissociation difference mass spectra (a) at 255 nm for $Mg^+(OCNC_2H_5)$, (b) at 339 nm for $Mg^+(OCNC_2H_5)_2$, and (c) at 414 nm for $Mg^+(OCNC_2H_5)_3$.

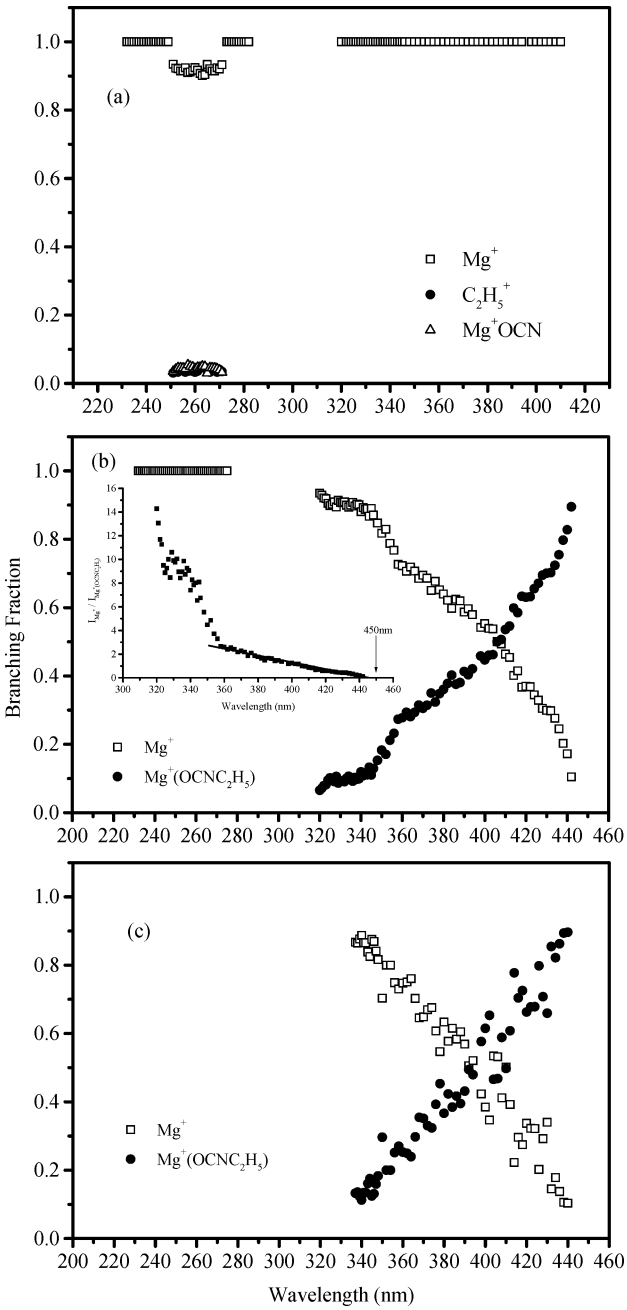

Figure 3. The branching fraction curves in the spectral range of 230−410 nm for $Mg^+(OCNC_2H_5)$ and 230−440 nm for $Mg^+(OCNC_2H_5)_{2-3}$. The inset in part b shows the intensity ratio of Mg^+ to $Mg^+(OCNC_2H_5)$ from photodissociation of $Mg^+(OCNC_2H_5)_2$ as a function of the laser wavelength.

on by the mass spectra with the photolysis laser off. The negative-going peak on the high mass side signifies the depletion of the mass-selected parent due to photodissociation, and the positive-going peaks indicate the appearance of the corresponding daughter ions. The branching fractions of the fragments as a function of the laser wavelength are shown in Figure 3 for $Mg^+(OCNC_2H_5)_{1-3}$. For the singly solvated cluster $Mg^+(OCNC_2H_5)$, the dominant photodissociation product is Mg^+, which results from nonreactive quenching throughout the entire wavelength range we studied (230−410 nm). The reactive products $C_2H_5^+$ and $Mg^+(OCN)$ are observed only at wavelengths shorter than ∼270 nm (∼4.59 eV). From energy consideration, the reactive channel for producing $C_2H_5^+$ (3.64 eV) and $Mg^+(OCN)$ (4.06 eV) from $Mg^+(OCNC_2H_5)$ is open in the shorter wavelength region (<270 nm, or >4.59 eV) based on our calculation. It is seen from Figure 3a that the branching ratios of Mg^+ to $C_2H_5^+$ and $Mg^+(OCN)$ are almost unchanged in the wavelength range 250−270 nm. This suggests that the reactions occur on the ground-state surface. The branching fraction curves for multisolvated complexes are different from that of the binary complex, suggesting that the photoinduced reaction patterns of large clusters $Mg^+(OCNC_2H_5)_n$ ($n > 1$) are not the same as are occurring in the photodissociation of the binary complex $Mg^+(OCNC_2H_5)$. For $Mg^+(OCNC_2H_5)_2$, as the wavelength decreases, the branching fraction of Mg^+ increases from zero at ∼440 nm to almost 100% at ∼320 nm (Figure 3b). Plotting the ratio of I_{Mg^+} versus $I_{Mg^+(OCNC_2H_5)}$ in the wavelength range of 320−440 nm (insert of Figure 3b), we obtain a lower appearance potential limit of the daughter cation Mg^+ of ∼450 nm (∼2.75 eV), which is to be compared with our calculated value of 2.78 eV. From the insert of Figure 3b, we noticed an interesting break near 360 nm. This break relates

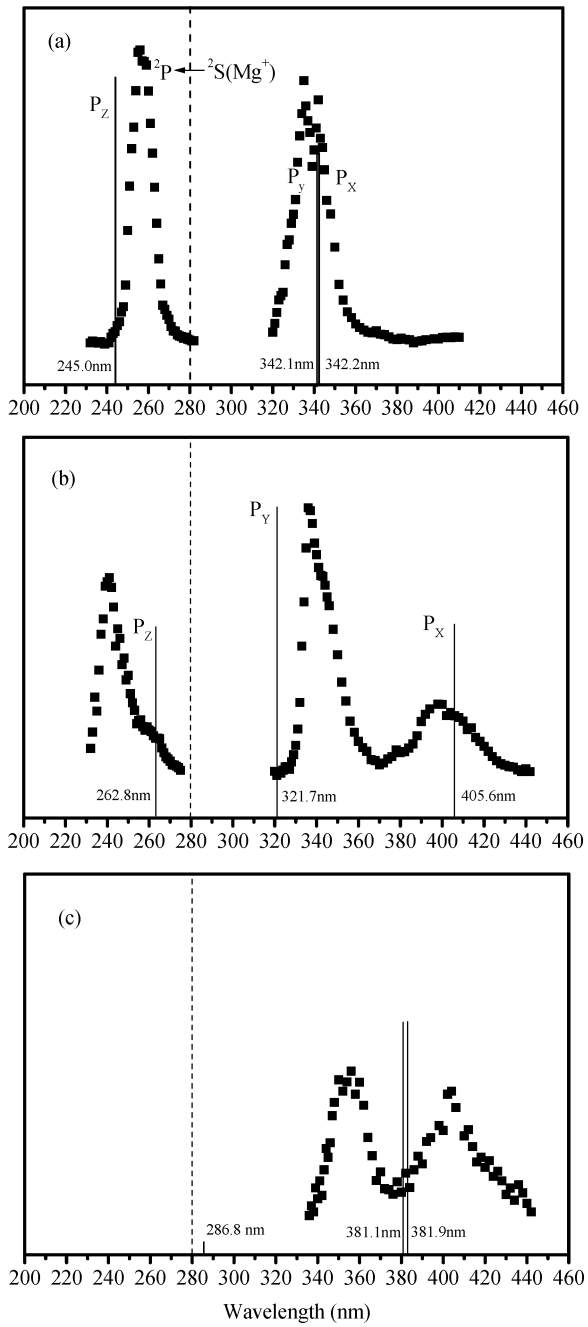

Figure 4. Action spectra of $Mg^+(OCNC_2H_5)_n$ ($n = 1-3$). The dashed line represents the atomic transition of Mg^+ ($^2P \leftarrow {}^2S$) at ~280 nm. The solid lines show the calculated absorption spectra for $Mg^+(OCNC_2H_5)_{1-3}$.

to the fact that the binding energies of the two solvent molecules ($OCNC_2H_5$) are different. Because the ion yield of $Mg^+(OCNC_2H_5)_2$ is very low, its branching fraction is not included in Figure 3c. For the multisolvated complexes $Mg^+(OCNC_2H_5)_n$ ($n \geq 2$), only nonreactive products were detected; two or three ethyl isocyanate molecules prefer evaporating together. This is partly due to the fact that the photon energies deposited in the complexes are sufficient to evaporate more than one solvent molecule.

Figure 4 shows the photodissociation action spectra of $Mg^+(OCNC_2H_5)_n$ ($n = 1-3$) in the wavelength range of 230−440 nm, in which the total fragment ion yields were normalized by the parent intensities and the photolysis laser fluence. The vertical dashed line at 280 nm represents the $3\ ^2P \leftarrow 3\ ^2S$ atomic transition of Mg^+. The vertical solid lines indicate the wavelengths and magnitudes of the calculated vertical transitions for $Mg^+(OCNC_2H_5)_n$ ($n = 1-3$). As seen in Figure 4a, there are two pronounced peaks in the photodissociation action spectrum of $Mg^+(OCNC_2H_5)$. These two peaks are centered at ~256 and ~340 nm, which are at the blue side and red side of the Mg^+ ($3\ ^2P \leftarrow 3\ ^2S$) atomic transition, respectively. For $Mg^+(OCNC_2H_5)_2$, besides two dominant peaks centered at ~240 and ~336 nm, a small bump centered at ~400 nm is also identified at the red side of the Mg^+ atomic transition. Only two peaks appear in the action spectrum of $Mg^+(OCNC_2H_5)_3$, situated at ~354 and ~404 nm, respectively. We failed to detect any ion signal at the blue side of the Mg^+ $3\ ^2P \leftarrow 3\ ^2S$ atomic transition. All the observed peaks in the action spectra are believed to originate from the $3\ ^2P \leftarrow 3\ ^2S$ transition of Mg^+. The splitting of the Mg^+ $3\ ^2P \leftarrow 3\ ^2S$ atomic transition is ascribed to the interactions between the three p orbitals of the excited Mg^+ and the orbitals derived from the NCO group of the ethyl isocyanate molecules. Such orbital interactions have been observed in previous photodissociation studies of many metal ion−molecule complexes.[8,18,41] The isocyano group O═C═N− is analogus to F^- as well as the cyano group N≡C−, but the action spectra of $Mg^+(OCNC_2H_5)_n$ ($n = 1-3$) are different from those of $Mg^+(FCH_3)_n$ ($n = 1-3$) or $Mg^+(NCCH_3)_n$ ($n = 1-3$) we reported previously.[8,18] The interpretation of the action spectra of $Mg^+(OCNC_2H_5)_n$ will be discussed in Section 3.3. combining with the theoretical calculations.

3.2. Ground-State Structures of $Mg^+(OCNC_2H_5)_n$ ($n = 1-3$). The ground-state geometries of the parent complexes $Mg^+(OCNC_2H_5)_n$ ($n = 1-3$) were fully optimized at the B3LYP/6-31+G** level by using the GAUSSIAN 98 package. The B3LYP/6-31+G** frequencies were used to calculated zero-point vibrational energies. The optimized structures were characterized by harmonic frequency analysis as local minima (all frequencies real). Extensive theoretical calculations on some alkaline earth metal cation−solvent complexes have been reported on both ground and excited states. For the ground states of the complexes, the calculated results are relatively accurate. The calculated structures for $Mg^+(OCNC_2H_5)_n$ ($n = 1-3$) are drawn in Figure 5. In Figure 5, the numbers between atoms represent the bond lengths, while those adjacent to atoms stand for the atomic charges. According to our calculations, the dipole moment of the ethyl isocyanate molecule is 3.317 D, which is almost the same as the previous value of 3.367 D given by Fehér et al.[27] In addition, from our B3LYP/6-31+G** calculations, the bond lengths of O═C, C═N, N−C, and C−C in the free $OCNC_2H_5$ molecule are found to be 1.184, 1.204, 1.451, and 1.526 Å, respectively, which are in reasonable agreement with previous experimental values ($r_{O=C} = 1.174$ Å, $r_{C=N} = 1.218$ Å, $r_{N-C} = 1.448$ Å, and $r_{C-C} = 1.524$ Å).[43] The calculated angles of ∠CCN (110.8°) and ∠OCN (173.5°) of the free ethyl isocyanate molecule are also quite close to the experimental values (114.7° and 167.8°, respectively).[43]

This work follows up on our previous report[40] and the structure for $Mg^+(OCNC_2H_5)$ is given here (Figure 5a) for comparison with that of $Mg^+(OCNC_2H_5)_{2-3}$. The geometry of $Mg^+(OCNC_2H_5)$ is characterized by bringing $OCNC_2H_5$ toward Mg^+ from the O end, and the resulting complex has an overall C_s symmetry. The $OCNC_2H_5$ molecule in the complex changes slightly except for the angle of ∠C2N3C4 (see Figure 6) and the charge distribution on the NCO part compared with the free $OCNC_2H_5$ molecule, which is consistent with the electrostatic nature of the bond between Mg^+ and $OCNC_2H_5$. In the free $OCNC_2H_5$ molecule, the N3 and O1 atoms adopt sp^2 hybridization, while the C2 atom adopts sp hybridization. The three sp^2-

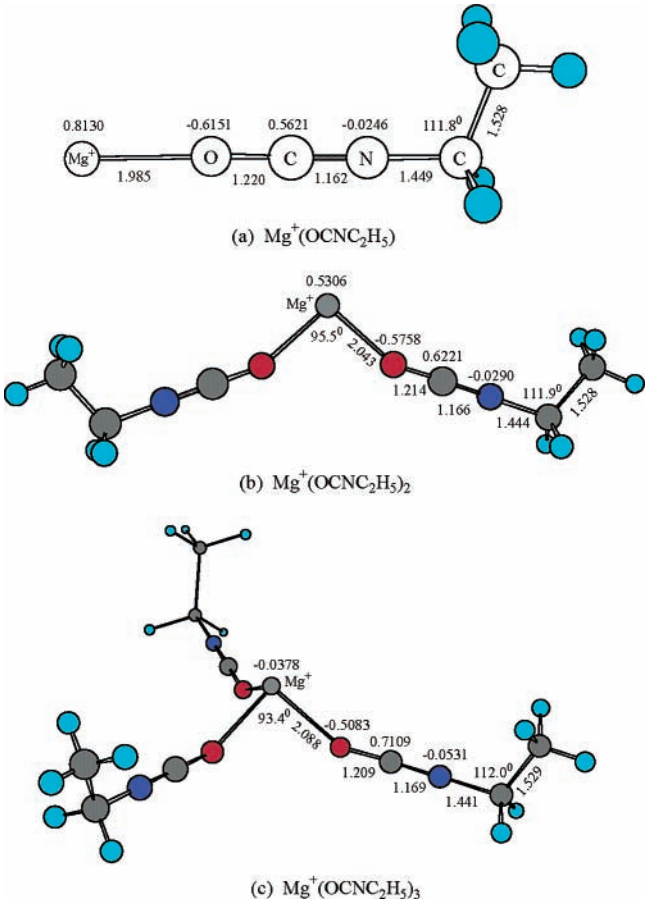

Figure 5. Optimized ground-state geometries for (a) $Mg^+(OCNC_2H_5)$, (b) $Mg^+(OCNC_2H_5)_2$, and (c) $Mg^+(OCNC_2H_5)_3$ at the B3LYP/6-31+G** level. The numbers between atoms represent the bond lengths, while those adjacent to atoms stand for the atomic charges.

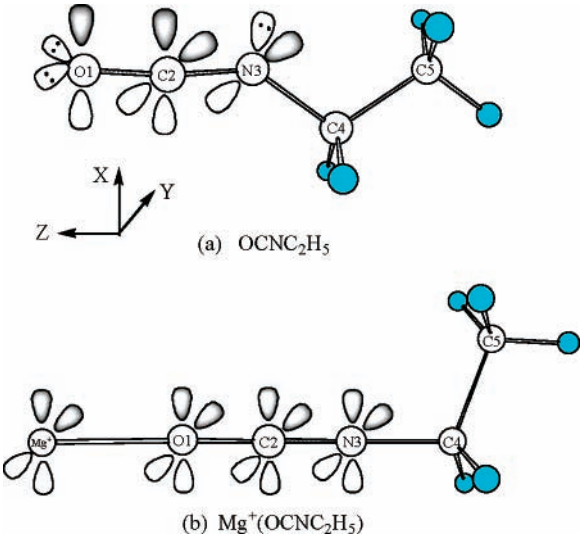

Figure 6. Schematic molecular orbital (MO) pictures for (a) $OCNC_2H_5$ and (b) $Mg^+(OCNC_2H_5)$.

hybridized orbitals of N3 lie in the *XZ* plane (see the coordinate designation in Figure 6); one is occupied by the lone-pair electrons of N3 and the others form two σ bonds with C2 and C4, respectively, rendering the stable bent structure ($\angle$C2N3C4 = 141.0°) of $OCNC_2H_5$. The p_y orbitals of N3 and C2 form a π bond lying in the *YZ* plane, while the p_x orbitals of C2 and O1 form another π bond in the *XZ* plane. These two π bonds are perpendicular to each other in the free $OCNC_2H_5$ molecule. During the complexation between the magnesium cation and the ethyl isocyanate molecule, not only Mg^+ undergoes sp hybridization, but also the hybridization methods in NCO group have changed. In the complex of $Mg^+(OCNC_2H_5)$, the N3 and O1 atoms also adopt sp hybridization as the C2 atom does due to the interaction with Mg^+. The two sp-hybridized oribals of each atom in the NCO group are used to form the σ bonds. The p_x orbitals of N3, C2, and O1 form a big π bond with the p_x orbital of Mg^+ lying in the *XZ* plane, while the p_y orbitals of N3, C2, and O1 form another big π bond with the p_y orbital of Mg^+ lying in the *YZ* plane. The sp hybridization occurring in the NCO group and the magnesium cation leads to an almost linear $Mg^+-O1-C2-N3-C4$ backbone structure. The formation of the two big π bonds in the complex of $Mg^+(OCNC_2H_5)$ due to the sp hybridization allows the charge to "move" between the NCO group and Mg^+. The sp hybridization of Mg^+ results in a high electron density located on the side of Mg^+ opposite to $OCNC_2H_5$, reducing the metal−ligand repulsion. The calculated minimum energy structure of $Mg^+(OCNC_2H_5)_2$ is shown in Figure 5b, in which the two $OCNC_2H_5$ molecules point from the O ends to the same side of Mg^+, as there is a high electron density on the other side of Mg^+. Only one stable structure was found for $Mg^+(OCNC_2H_5)_3$ (Figure 5c); all three $OCNC_2H_5$ molecules are directly linked to Mg^+ from the O ends, and on the same side to minimize the electron repulsion from the high electron density on the other side of Mg^+.

On the basis of our calculations (see Figure 5), there are some noticeable changes in the complexes of $Mg^+(OCNC_2H_5)_n$ ($n = 1-3$) during the solvation of Mg^+ by the ethyl isocyanate molecule. First of all, a large increment of the Mg^+-O bond distance (~0.05 Å) is found from $Mg^+(OCNC_2H_5)$ to $Mg^+(OCNC_2H_5)_3$. In $Mg^+(OCNC_2H_5)_n$, the interaction between the magnesium cation and the ethyl isocyanate molecule is mainly of electrostatic nature. An sp hybridization in the complexation of Mg^+ and $OCNC_2H_5$ takes place to reduce the metal−ligand repulsion, resulting in a high electron density located on the side of Mg^+ opposite from $OCNC_2H_5$. When there is further solvation of Mg^+ by the $OCNC_2H_5$ molecule, because there is a high electron density on the other side of Mg^+, the ethyl isocyanate molecules are all on the same side of Mg^+ to minimize the electron repulsion from the other side of Mg^+. The consequence of this arrangement leads to the ligand−ligand repulsion becoming larger and larger as the solvent molecule accumulates. Second, an almost identical decrease of the O=C bond is observed for all the complexes of $Mg^+(OCNC_2H_5)_{1-3}$, e.g., a decrease by 0.006 Å from $Mg^+(OCNC_2H_5)$ to $Mg^+(OCNC_2H_5)_2$ and 0.005 Å from $Mg^+(OCNC_2H_5)_2$ to $Mg^+(OCNC_2H_5)_3$. Similarly, a gradual decrease (0.005−0.003 Å) of the N−C bond between NCO and ethyl groups is also observed from $Mg^+(OCNC_2H_5)$ to $Mg^+(OCNC_2H_5)_3$. Furthermore, an increment (0.004−0.003 Å) of the C=N bond in the NCO group is found for the complexes $Mg^+(OCNC_2H_5)_n$ from $n = 1$ to 3. The change of the bond lengths in the ethyl isocyanate part mentioned above indicates that the interaction between Mg^+ and the lone-pair electrons of O in the complexes of $Mg^+(OCNC_2H_5)_n$ is transmitted from O to C, to N, and to N−C bond through conjugation. In other words, the NCO group acts as an atom as it should be for a halogen analogue. A similar situation was also observed in our previous work on $Mg^+(NCCH_3)_n$ ($n = 1-4$).[8] Finally, a remarkable change of the atomic charges in the complexes $Mg^+(OCNC_2H_5)_n$ ($n = 1-3$) should not be ignored. It is seen in Figure 5 that with the accumulation of ethyl isocyanate molecules around the Mg^+ core, the atomic charge of Mg^+

TABLE 1: Calculated Total Energies and Binding Energies, Using B3LYP/6-31+G for $Mg^+((ocnc_2H_5)_n$ ($n = 1-3$)[a]**

complexes	calculated energy (hartree)
$OCNC_2H_5$	−247.243370
$Mg^+(OCNC_2H_5)$	−447.100912
$Mg^+(OCNC_2H_5)_2$	−694.384344
$Mg^+(OCNC_2H_5)_3$	−941.655406
$Mg^+(OCNC_2H_5) \rightarrow Mg^+ + OCNC_2H_5$	$\Delta E_{cal} = 1.69$ eV (38.9 kcal/mol)
$Mg^+(OCNC_2H_5)_2 \rightarrow Mg^+(OCNC_2H_5) + OCNC_2H_5$	$\Delta E_{cal} = 1.09$ eV (25.1 kcal/mol)
$Mg^+(OCNC_2H_5)_3 \rightarrow Mg^+(OCNC_2H_5)_2 + OCNC_2H_5$	$\Delta E_{cal} = 0.75$ eV (17.4 kcal/mol)

[a] All the energies include the zero-point energy corrections.

becomes less and less positive. For $Mg^+(OCNC_2H_5)_3$, the atomic charge of magnesium experiences a sign change to negative (−0.0378), while in the NCO group of the complexes of $Mg^+(OCNC_2H_5)_{1-3}$, the charge on the O atom becomes less and less negative as n increases. Analyzing the change of the calculated atomic charges in $Mg^+(OCNC_2H_5)_n$ ($n = 1-3$), one notices that the magnesium acts as an electron acceptor and the isocyanate acts as an electron donor through the O end.

Binding energies of $Mg^+(OCNC_2H_5)_n$ ($n = 1-3$) for the first ethyl isocyanate are listed in Table 1. All the energies listed in Table 1 include the zero-point energy corrections. The binding energy of a given cation−molecule complex was calculated as the difference between the total energy of the complex in its optimized ground-state geometry, $E[Mg^+(OCNC_2H_5)_n]$, and the total energies of $Mg^+(OCNC_2H_5)_{n-1}$ and $OCNC_2H_5$ in the gas phase, $E[Mg^+(OCNC_2H_5)_{n-1}] + E[OCNC_2H_5]$. The successive solvation energies decrease with the increasing cluster size although the extent of the decrease becomes smaller and smaller. For example, the binding energy of $Mg^+(OCNC_2H_5)$ is 38.9 kcal/mol (1.69 eV), and decreases to 25.1 (1.09 eV) and 17.4 kcal/mol (0.75 eV) for $Mg^+(OCNC_2H_5)_2$ and $Mg^+(OCNC_2H_5)_3$, respectively. The ground-state binding energy of $Mg^+(OCNC_2H_5)$ is larger than that of $Mg^+(FCH_3)$ (26.8 kcal/mol or 1.06 eV),[18] but is smaller than that of $Mg^+(NCCH_3)$ (42.4 kcal/mol or 1.84 eV).[8] Similar to acetonitrile, which is an aprotic solvent molecule ($\mu = 3.92$ D),[8] ethyl isocyanate also possesses a relatively large dipole moment ($\mu = 3.367$ D),[27] while the dipole moment of FCH_3 is only 1.858 D.[18] Therefore, the charge−dipole interaction between the magnesium cation and the ethyl isocyanate molecule is significantly enhanced in $Mg^+(OCNC_2H_5)$. Moreover, the orbitals derived from the NCO group also interact with the p orbitals of Mg^+, resulting in an additional enhancement in binding energy.

3.3. Action Spectra of $Mg^+(OCNC_2H_5)_n$. On the basis of the theoretical calculations for the ground state, vertical excitation energies to the lowest excited states of $Mg^+(OCNC_2H_5)_n$ ($n = 1-3$) were calculated by using a less extended CI referred to as the CI-single (CIS) approach. The basis set of 6-31+G** was also used in this calculation. The calculated absorption spectra of $Mg^+(OCNC_2H_5)_n$ ($n = 1-3$) are graphically shown by the solid lines in Figure 4 along with the experimental data. For comparison, the atomic transition of Mg^+ ($3\,^2P \leftarrow 3\,^2S$) at 280 nm is also shown by the dashed line in Figure 4. The locations of the solid lines represent the excitation energies and the amplitudes indicate the oscillator strengths for the transitions. Although the calculated absorption spectrum of $Mg^+(OCNC_2H_5)_3$ does not seem to tally with that of the action spectrum, for $Mg^+(OCNC_2H_5)_{1-2}$, the calculated vertical transitions agree well with the experimental action spectra. The CIS calculation only considers single excitations and does not describe adequately the states with significant double excitation. Therefore, for the excited states, the calculated results can only provide some reasonable explanations of experimental results. Especially, caution should be taken for the calculations on large complexes. It is seen in Figure 4 that the spectral features of $Mg^+(OCNC_2H_5)_n$ are derived from the atomic transition of Mg^+ ($3\,^2P \leftarrow 3\,^2S$) with significant perturbation by the presence of $OCNC_2H_5$ molecules. The magnitude of the peak splitting depends on the orientations of the three $3p_{x,y,z}$ orbitals of magnesium cation with respect to the solvent arrangements around Mg^+.

For the two excited states $3\,^2P_{X,Y}$ of $Mg^+(OCNC_2H_5)$ (see the coordination in Figure 5a or Figure 6), the two $3p_{x,y}$ orbitals of Mg^+ are perpendicular to the Mg^+-O bond axis. The presence of the two antibonding π^* orbitals of the NCO group reduces electron density along the Mg^+-O bond, and hence the repulsion, leading to the energies of $3\,p_{x,y}$ being lowered, which accounts for the large red shift of the relative broad peak in the action spectrum of $Mg^+(OCNC_2H_5)$. In the excited state $3\,^2P_z$ of $Mg^+(OCNC_2H_5)$, the p_z orbital of Mg^+ is oriented along the Mg^+-O bond axis. The strong repulsive interaction between the parallel $3p_z$ electron of Mg^+ and the lone-pair electrons of O lifts the energy of the p_z orbital. So the $3\,^2P_z$ state is blue-shifted relative to the atomic transition of Mg^+ ($3\,^2P \leftarrow 3\,^2S$) as observed. According to our calculations, the Mg^+-O-C angle of the ground-state $Mg^+(OCNC_2H_5)$ is 178.5°, and the angles of O−C−N and C−N−C are 179.8° and 179.1°, respectively, which render a nearly linear backbone of $Mg^+-O-C-N-C$ in $Mg^+(OCNC_2H_5)$. Therefore, the $3\,^2P_x$ and $3\,^2P_y$ states are almost degenerate and are nearly superpositioned in the action spectrum of $Mg^+(OCNC_2H_5)$ (Figure 4a). On the basis of the above consideration, the relative broad red peak (320−360 nm) in the action spectrum of $Mg^+(OCNC_2H_5)$ is assigned to the transitions to the $3\,^2P_x$ ($2\,^2A'$) and $3\,^2P_y$ ($1\,^2A''$) excited states (based on C_s symmetry). The sharp blue peak centered at ∼256 nm is ascribed to the transition to $3\,^2P_z$ ($3\,^2A'$) state. The two adjacent excited states $2\,^2A'$ and $1\,^2A''$ result from the electron promotion from the 3s orbital to the $3p_{x,y}$ orbitals of Mg^+, while in the excited state $3\,^2A'$, the $3p_z$ orbital is occupied by an electron excited from the 3s orbital.

The action spectrum of $Mg^+(OCNC_2H_5)_2$ (Figure 4b) differs significantly from that of $Mg^+(OCNC_2H_5)$ (Figure 4a). Three well-separated peaks can be identified in the action spectrum. The small bump centered at ∼400 nm (Figure 4b) is ascribed to the $3\,^2P_X$ state (see the coordination in Figure 5b), in which the $3p_x$ orbital of Mg^+ interacts with two big antibonding π^* orbitals of the two NCO groups in $Mg^+(OCNC_2H_5)_2$. The in-phase interaction with the two empty antibonding π^* orbitals lowers the energy level of the p_x orbital of the magnesium cation significantly, resulting in the large red-shift compared with the atomic transition of Mg^+ ($3\,^2P \leftarrow 3\,^2S$). The peak centered at ∼240 nm is the contribution from the state of $3\,^2P_Z$, in which the $3p_z$ orbital of Mg^+ interacts repulsively with the nonbonding electrons of O atoms of the NCO group in $Mg^+(OCNC_2H_5)_2$. Therefore, the repulsion between the $3p_z$ electron of Mg^+ and the lone-pair electrons of the two O atoms lifts the energy of the $3p_z$ orbital of Mg^+, resulting in the $3\,^2P_Z$ state blue-shifted in the action spectrum of $Mg^+(OCNC_2H_5)_2$. The highest peak

centered at ~336 nm is assigned to the 3 ^2P_Y excited state. In the 3 ^2P_Y state, the interaction between the $3p_y$ orbital of Mg^+ and the two big antibonding π^* orbitals of the NCO groups is not intensive, and the energy of the $3p_y$ orbital is not lowered much compared with that of the $3p_x$ orbital of Mg^+. So the transition to the 3 ^2P_Y state is between the atomic transition of Mg^+ (3 $^2P \leftarrow 3\ ^2S$) and the transition to the 3 ^2P_X state.

The optimized ground-state geometry of $Mg^+(OCNC_2H_5)_3$ shown in Figure 5c has nearly a C_{3v} symmetry. The *XY* plane is parallel to the plane formed by the three O atoms. The repulsive interactions between the $3p_{x,y}$ orbitals of Mg^+ and the three O atoms are similar, giving rise to two closely spaced states 3 ^2P_X and 3 ^2P_Y. In the $Mg^+(H_2O)_n$ systems,[23b] Fuke et al. observed a very small splitting for $Mg^+(H_2O)_3$ compared with those for $Mg^+(H_2O)$ and $Mg^+(H_2O)_2$ and gave a reasonable explanation. According to ab initio calculations, $Mg^+(H_2O)_3$ has an equilibrium structure with C_{3v} symmetry in which three equivalent waters all bind to the side of Mg^+. The three pπ-like states of $Mg^+(H_2O)_3$ are destabilized by metal−ligand interaction with nearly the same ammount, leading to much closer excitation energies for the three excited states. They assigned the two close bands of $Mg^+(H_2O)_3$ from the three p $\leftarrow$ s-type transitions. A similar situation also occurred in $Mg^+(CH_3OH)_n$ systems.[16] Farrar and co-workers observed a single strong band in the longer wavelength region and a weak bump in the shorter area. These results may suggest that the two adjacent peaks centered at ~354 and ~404 nm, respectively, in the action spectrum of $Mg^+(OCNC_2H_5)_3$ in the longer wavelength region include the P_z transition.

Theoretical and experimental study shows that the metal−ligand interaction is due mainly to charge−dipole interaction in metal ion−molecule complexes. The consequence of this interaction gives rise to a relatively high electron density on the other side of the metal ion opposite to the "bond" of the metal−ligand. In solvation, the successive solvent molecules incline to bind to metal ion on the same side to minimize the electron repulsion. With the number of ligands increasing, the ligand−ligand repulsive interaction is enhanced. As more ligands are attached to the metal ion, the structure of the complex becomes more and more "planar" and the complex becomes more and more stablized. However, there is a limit to how far the complex can go toward the "planar" structure because the solvent molecules prefer staying on the same side of the metal ion. This is partially the reason that the intensities of $Mg^+(OCNC_2H_5)_n$ ($n \geq 3$) are relatively low.

4. Conclusion

(1) This study has extended our recent work[40] on the photodissociation of $Mg^+-OCNC_2H_5$. The metal cation−molecule complexes $Mg^+(OCNC_2H_5)_n$ ($n = 1-6$) have been produced in a laser-ablation supersonic expansion nozzle source. The relative photodissociation product yields as a function of the excitation wavelength in the spectral range of 230−440 nm have been measured by mass-selecting each complex of $Mg^+(OCNC_2H_5)_{1-3}$.

(2) Except for the reaction products $C_2H_5^+$ and Mg^+OCN with low yields at short wavelengths from the photodissociation of $Mg^+(OCNC_2H_5)$, only evaporation products were observed from photodissociation of all three complexes. The appearance potential of Mg^+ from photodissociation of $Mg^+(OCNC_2H_5)_2$ is deduced to be ~450 nm (~2.75 eV) on the basis of the branching fraction curves of $Mg^+(OCNC_2H_5)_2$, which agrees well with our calculated value of 2.78 eV.

(3) Through theoretical calculations at the B3LYP/6-31+G** level with use of the GAUSSIAN 98 package, the ground-state structures of the complexes $Mg^+(OCNC_2H_5)_n$ ($n = 2-3$) have been determined. Vertical excitation energies to the lowest excited states of $Mg^+(OCNC_2H_5)_{2-3}$ were calculated on the basis of the optimized geometries of their ground states. The calculated absorption spectrum of $Mg^+(OCNC_2H_5)_2$ calculated by using the optimized geometries of its ground state accords well with the observed action spectrum in terms of both the positions and amplitudes.

(4) The change of hybridization path of atomic orbitals took place when the magnesium cation complexed with the ethyl isocyanate molecule. Based on sp hybridization, we advanced a big π-bond system for the complexation between Mg^+ and $OCNC_2H_5$, which rationalized the nearly linear backbone of $Mg^+-O-C-N-C$ in the complex of $Mg^+(OCNC_2H_5)$.

Acknowledgment. This work was supported by an RGC grant administered by the UGC of Hong Kong. Ke-Li Han also thanks the support from a NKBRSF grant (G1999075302) and NSFC (20333050).

References and Notes

(1) Duncan, M. A. *Annu. Rev. Phys. Chem.* **1997**, *48*, 69.
(2) Misaizu, F.; Sanekata, M.; Fuke, K.; Iwata, S. *J. Chem. Phys.* **1994**, *100*, 1161.
(3) Shen, M. H.; Farrar, J. M. *J. Phys. Chem.* **1989**, *93*, 4386.
(4) Sperry, D. C.; Midey, A. J.; Lee, J. I.; Qian, J.; Farrar, J. M. *J. Chem. Phys.* **1999**, *111*, 8469.
(5) Rodgers, M. T.; Armentrout, P. B. *J. Am. Chem. Soc.* **2000**, *122*, 8548.
(6) Armentrout, P. B.; Rodgers, M. T. *J. Phys. Chem. A* **2000**, *104*, 2238.
(7) Elhanine, M.; Dukan, L.; Maître, P.; Breckenridge, W. H.; Massick, S.; Soep, B. *J. Chem. Phys.* **2000**, *112*, 10912.
(8) Liu, H.; Guo, W.; Yang, S. *J. Chem. Phys.* **2001**, *115*, 4612.
(9) Kleiber, P. D.; Chen, J. *Int. Rev. Phys. Chem.* **1998**, *17*, 1.
(10) Ding, L. N.; Kleiber, P. D.; Cheng, Y. C.; Young, M. A.; Oneil, S. V.; Stwalley, W. C. *J. Chem. Phys.* **1995**, *102*, 5235.
(11) Sanekata, M.; Misaizu, F.; Fuke, K. *J. Chem. Phys.* **1996**, *104*, 9768.
(12) Yoshida, S.; Okai, N.; Fuke, K. *Chem. Phys. Lett.* **2001**, *347*, 93.
(13) Yeh, C. S.; Pilgrim, J. S.; Willey, K. F.; Robbins, D. L.; Duncan, M. A. *Int. Rev. Phys. Chem.* **1994**, *13*, 231.
(14) Bauschlicher, C. W., Jr.; Sodupe, M.; Partridge, H. *J. Chem. Phys.* **1992**, *96*, 4453.
(15) Shen, M. H.; Farrar, J. M. *J. Chem. Phys.* **1991**, *94*, 3322.
(16) Lee, J. I.; Sperry, D. C.; Farrar, J. M. *J. Chem. Phys.* **2001**, *114*, 6180.
(17) Lu, W.; Yang, S. *J. Phys. Chem. A* **1998**, *102*, 825.
(18) Yang, X.; Liu, H.; Yang, S. *J. Chem. Phys.* **2000**, *113*, 3111.
(19) Märk, T. D.; Castleman, A. W., Jr. *Adv. At. Mol. Phys.* **1985**, *30*, 65.
(20) Castleman, A. W., Jr.; Keesee, R. G. *Chem. Rev.* **1986**, *86*, 589.
(21) Stein, G. D. *Phys. Technol.* **1979**, *17*, 503.
(22) Castleman, A. W., Jr.; Wei, S. *Annu. Rev. Phys. Chem.* **1994**, *45*, 685.
(23) (a) Misaizu, F.; Sanekata, M.; Tsukamoto, K.; Fuke, K.; Iwata, S. *J. Phys. Chem.* **1992**, *96*, 8259. (b) Misaizu, F.; Sanekata, M.; Tsukamoto, K.; Fuke, K.; Iwata, S. *J. Chem. Phys.* **1994**, *100*, 1161. (c) Watanabe, H.; Iwata, S.; Hashimoto, K.; Misaizu, F.; Fuke, K. *J. Am. Chem. Soc.* **1995**, *117*, 755.
(24) (a) Willey, K. F.; Yeh, C. S.; Robbins, D. L.; Pilgrim, J. S.; Duncan, M. A. *Int. J. Mass. Spectrom. Ion Processes* **1992**, *97*, 8886. (b) Scurlock, C. T.; Pullins, S. H.; Reddic, J. E.; Duncan, M. A. *J. Chem. Phys.* **1996**, *104*, 4591.
(25) Sodupe, M.; Bauschlicher, C. W., Jr. *Chem. Phys. Lett.* **1992**, *195*, 494.
(26) (a) Shen, M. H.; Farrar, J. M. *J. Phys. Chem.* **1989**, *93*, 3322. (b) Donnelly, S. G.; Farrar, J. M. *J. Chem. Phys.* **1993**, *98*, 5450. (c) Qian, J.; Midey, A. J.; Donnelly, S. G.; Lee, J. I.; Farrar, J. M. *Chem. Phys. Lett.* **1995**, *244*, 414.
(27) Fehér, M.; Pasinszki, T.; Veszprémi, T. *J. Am. Chem. Soc.* **1993**, *115*, 1500.
(28) Sullivan, J. F.; Durig, D. T.; Durig, J. R.; Cradock, S. *J. Phys. Chem.* **1987**, *91*, 1770.

(29) Karpas, Z.; Stevens, W. J.; Buckley, T. J.; Metz, R. *J. Phys. Chem*. **1985**, *89*, 5274.
(30) Pasinszki, T.; Westwood, N. P. C. *J. Phys. Chem*. **1995**, *99*, 1649.
(31) Stevens, J. E.; Cui, Q.; Morokuma, K. *J. Chem. Phys*. **1998**, *108*, 1452.
(32) Pasinszki, T.; Westwood, N. P. C. *J. Phys. Chem. A* **2001**, *105*, 1244.
(33) Paul, D. K.; Marten, C. D. *Langmuir* **1998**, *14*, 3820.
(34) Ozensoy, E.; Hess, C.; Goodman, D. W. *J. Am. Chem. Soc*. **2002**, *124*, 8524.
(35) Klapotke, T. M.; Schulz, A. *Inorg. Chem*. **1996**, *35*, 7897.
(36) Bion, N.; Saussey, J.; Seguelong, T.; Daturi, M. *Phys. Chem. Chem. Phys*. **2001**, *3*, 4811.
(37) Wang, X.; Zhou, M.; Andrews, L. *J. Phys. Chem. A* **2000**, *104*, 10104.
(38) Armentrout, P. B.; Tjelta, B. L. *Organometallics* **1997**, *16*, 5372.
(39) Paul, D. K.; McKee, M. L.; Worley, S. D.; Hoffman, N. W.; Ash, D. H.; Gautney, J. *J. Phys. Chem*. **1989**, *93*, 4598.
(40) Sun, J. L.; Liu, H.; Han, K. L.; Yang, S. *J. Chem. Phys*. **2003**, *118*, 10455.
(41) (a) Yang, X.; Hu, Y. H.; Yang, S. H. *Chem. Phys. Lett*. **2000**, *322*, 491. (b) Yang, X.; Hu, Y. H.; Yang, S. H. *J. Phys. Chem. A* **2000**, *104*, 8496. (c) Yang, X.; Gao, K. L.; Liu, H. C.; Yang, S. H. *J. Chem. Phys*. **2000**, *112*, 10236.
(42) Ohshimo, K.; Tsunoyama, H.; Yamakita, Y.; Misaizu, F.; Ohno, K. *Chem. Phys. Lett*. **1999**, *301*, 356.
(43) Cradock, S.; Durig, J. R.; Sullivan, J. F. *J. Mol. Struct*. **1985**, *131*, 121.